Available online at www.sciencedirect.com
ScienceDirect
Journal of the European Ceramic Society 30 (2010) 37–52
www.elsevier.com/locate/jeurceramsoc

Red ceramic pigments of terbium-doped ceria prepared through classical and non-conventional coprecipitation routes

M. Llusar [a,*], L. Vitásková [b], P. Šulcová [b], M.A. Tena [a], J.A. Badenes [a], G. Monrós [a]

[a] *Departamento de Química Inorgánica y Orgánica, Universitat Jaume I, 12071 Castellón, Spain*
[b] *Faculty of Chemical Technology, University of Pardubice, Legions Sqr. 565, 53210 Pardubice, Czech Republic*

Received 20 May 2009; received in revised form 23 July 2009; accepted 6 August 2009
Available online 8 September 2009

Abstract

Reddish ceramic pigments based on cerianite compositions $Ce_{1-x}Tb_xO_2$ ($x = 0.1$, 0.2 and 0.3) and $Ce_{0.9}Tb_{0.05}Y_{0.05}O_2$ have been prepared. Firstly, the optimal composition giving the best red colour was selected ($Ce_{0.9}Tb_{0.1}O_2$) from ceramic and chlorides coprecipitation samples fired at 1100–1500 °C. Secondly, the effect of using different classical and non-conventional coprecipitation routes on the synthesis and colouring performance of CeO_2-Tb red pigments was analyzed for the first time. In addition to classical coprecipitation we tested also the use of hydrothermal treatment and other more homogeneous coprecipitation methods with oxalates and urea. Homogeneous coprecipitation was also combined with ultrasonic or microwave irradiation. Samples were characterized by thermal analysis, XRD, SEM/EDX, optical spectroscopy and colour measurements. Interestingly, the optimization of synthesis methods enabled to obtain more homogeneous (single phase) CeO_2-Tb solid solutions at lower temperatures (400–1100 °C), exhibiting very nice reddish colourations associated to lower energy bandgaps (E_g below 2.30 eV). The obtained optimal compositions could be therefore alternative candidates as environmentally friendly reddish ceramic pigments.

Keywords: A. Sol–gel processes; C. Colour; C. Optical properties; D. CeO_2; E. Red ceramic pigments

1. Introduction

Many investigations are concerned to ceria (CeO_2)-based materials given their interesting ionic conductivity (labile oxygen vacancies) and catalytic properties. Both properties arise from the mixed valence of cerium (Ce^{3+}/Ce^{4+}) and the flexibility of the adopted fluorite structure,[1–3] and can be smartly tuned or enhanced by doping ceria with rare earths (*i.e.* Eu, Pr, Tb, Sm, Gd, etc.) and other transition or main group metals (*i.e.* Cr, Ti, Zr, Y, Pt, Rh, Ca or In). Accordingly, ceria-based solid solutions have found many advanced technologic applications, as three-way catalysts (TWCs) for automotive exhausts,[4,5] support or active catalysts,[6,7] gas sensors and solid oxide fuel cells (SOFCS),[8–10] photoluminescent materials,[11] and other electroceramic materials.

On the other hand, Pr-doped ceria is also employed in the ceramic industry since 1960 as red ceramic pigment.[12] In response to growing concerns demanding environmentally benign (and commercially viable) ceramic pigments,[13–18] Pr-CeO_2 and related ceria-based solid solutions have become interesting low-toxicity alternatives[19–24] to other traditionally used orange-red ceramic pigments. Indeed, the choice of available reddish ceramic pigments is restricted either to pigments involving toxicity problems (associated to Cd, Pb and Cr), such as $CdS_{1-x}Se_x$ (in a zircon matrix), Pb_3O_4 (in tin oxide matrixes) or $Ln_x(Al_{2-x-y}Cr_y)O_3$ perovskites,[21,25–29] or to pigments which lack of sufficient colour purity and reproducibility, such as α-Fe_2O_3 included in a zircon matrix.[30]

Different aspects of Pr-CeO_2 system have been profusely investigated in the last decade (synthesis, microstructure, oxidation states, crystallographic and colouring properties, etc.). In these studies the pigmenting solid solutions were prepared by the ceramic method[19–21,31–34] and also through many other non-conventional routes (*i.e.* coprecipitation of hydroxides, oxalates or carbonates, urea homogeneous coprecipitation, flux method, combustion, pirolysis, hydrothermal or microwave-

* Corresponding author at: Departament de Química Inorgànica y Orgànica, Universitat Jaume I, Edifici Científico-Tècnic, Av. Sos Baynat s/n, 12071 Castellón, Spain. Tel.: +34 964 728244; fax: +34 964 728214.
E-mail address: mllusar@qio.uji.es (M. Llusar).

0955-2219/$ – see front matter © 2009 Elsevier Ltd. All rights reserved.
doi:10.1016/j.jeurceramsoc.2009.08.005

assisted hydrothermal, and so forth).[1,2,5,21,33,35–41] Noteworthy, previous investigations have demonstrated that ceramic pigments based on Tb-CeO_2 solid solutions may also yield good red hues,[20,21,42,43] which may be comparable to those obtained with Pr-CeO_2. Nevertheless, the studies about synthesis optimization and pigmenting properties of Tb-doped ceria are still rather scarce, since most of research concerning this system is centred on catalytic or redox properties.[4,6,11] As far as we are concerned, the available investigations involve only compositions prepared by the ceramic method[20,42] or by calcination of hydroxides[21,42,43] or oxalates coprecipitates.[42] In the last case, however, the synthesis of the samples was not described by the authors. Thus, further studies are still needed to optimize the synthesis conditions and colour properties of Tb-CeO_2 red ceramic pigments, which could be an interesting alternative to the Pr-CeO_2 system.

In this work we analyze for the first time the effect of using different classical and non-conventional coprecipitation routes on the low-temperature synthesis and colour performance of Tb-CeO_2 red pigments. The optimization of synthesis methods may enable the formation of more homogeneous (single phase) Tb-CeO_2 solid solutions at lower temperatures. Moreover, the employed synthesis method may affect the final Ce–O and Tb–O chemical environments in the pigment (lattice parameters and volume and the optical bandgap), thus affecting the final reddish colouration. In addition to classical coprecipitation of hydroxides with ammonia, which often leads to heterogeneous and coarse precipitate particles, herein we have also tested the use of hydrothermal treatment and other more homogeneous coprecipitation methods (with oxalates and urea). Hydrothermal treatment applied to freshly prepared colloidal coprecipitates may enable the formation of high-purity and fine-grained powders at lower temperatures.[40] On the other hand, the use of more homogeneous precursors through the precipitation of a mixed oxalate[31] or also through urea-based (or hexamethylentetramine-based) homogenous precipitation[1,44,45] may result in the formation of pure and more homogenous solid solutions at lower temperatures (1100 °C or below), and improve the colouring performance.

As another two less conventional routes, homogeneous coprecipitation was also combined with the assistance of ultrasonic or microwave irradiation treatments.[46] Sonochemical synthesis (sonocoprecipitation) is becoming a routine method for preparing nanostructured materials.[47–49] The chemical effects of ultrasonic irradiation (originated from acoustic cavitation phenomena) provide high local temperatures and pressures, which could enhance reactivity and lead to well-dispersed, non-agglomerated colloidal powders.[50] Microwave-assisted hydrothermal synthesis, on the other hand, has been already applied to Pr-CeO_2[40,41] and other pigmenting systems.[51] This method enables the rapid formation of homogenous and ultrafine powders, and is highly advantageous in terms of cost and energy savings due to the shorter processing times and the higher reaction rates to form the target material.[40,52]

The formation and chemical homogeneity of Tb-CeO_2 solid solutions has been followed by XRD, cell parameters measurement, and SEM/EDX characterization, while the colour performance as red ceramic pigments has been analyzed through reflectance diffuse spectroscopy and colour measurements.

2. Experimental procedure

2.1. Sample preparation

In a preliminary study (optimization of composition), ceramic samples with compositions $Ce_{1-x}Tb_xO_2$ ($x = 0.1$, 0.2 and 0.3) and $Ce_{0.9}Tb_{0.05}Y_{0.05}O_2$ (from now on, compositions with $x = 0.05$) were prepared by ball-milling mixtures of the corresponding oxide precursors (CeO_2, 99.9%; Tb_4O_7 99.9%; Y_2O_3 99,9%; all from *Strem Chemicals Inc.*), and subsequent calcination at different final temperatures (1100 °C/6 h, 1300 °C/1 h and 1500 °C/1 h) in an electrical furnace. H_3BO_3 (99.5%, J. T. Baker) was also added as flux agent or mineralizer (2 wt% addition) in some compositions ($x = 0.05$ and 0.1) to analyze its effect on solid-state reaction. To select the optimal composition, coprecipitate samples with similar compositions and firing treatments were also prepared, using chloride salts as precursors (COCl samples). In these samples a mineralized composition was also prepared only for $x = 0.05$ (2 wt% addition of H_3BO_3 to the dried coprecipitate).

As the main focus of the investigation (optimization of synthesis method), in the second part samples with the selected optimal composition ($x = 0.1$—$Ce_{0.9}Tb_{0.1}O_2$—and without H_3BO_3) were then prepared through different classical and non-conventional coprecipitation routes, as previously indicated in the introduction. Table 1 summarizes the information about samples nomenclature, precursors and the employed preparation conditions.

All the as-prepared coprecipitate powders were fired at lower temperatures (400, 600 and 1100 °C, with 6 h of soaking time) to analyze the early crystallization and homogeneity of CeO_2-Tb solid solutions, and the production of interesting red hues at much lower temperatures than samples prepared by the ceramic method (1100–1500 °C).

2.2. Sample characterization

Simultaneous differential thermal and thermogravimetric analysis (DTA-TGA) of dried coprecipitates was carried out with a Mettler Toledo thermal analyzer (using Pt crucibles with a constant 5 °C/min heating from 25 up to 1200 °C). Crystallochemical characterization of calcined samples was performed by X-ray diffraction (XRD) in a Siemens D-500 powder Diffractometer with Ni-filtered CuK_α radiation (from 10 to 70°2θ, with steps of 0.02°2θ and a counting time of 2 s/step). For the calculation of cell parameters, much slower XRD runs using corundum as internal standard (40 wt%) were carried out (this time from 24 to 80°2θ, with steps of 0.02°2θ and a counting time of 4 s/step), and the obtained XRD patterns were refined and analyzed with TREOR[53] and Win-metric[54] programs.

On the other hand, the morphology and microstructure of CeO_2-Tb solid solutions obtained after calcination was examined by scanning electron microscopy (SEM) with a Leo-440i

Table 1
Nomenclature, precursors (or other additives) and preparation conditions in the synthesis of coprecipitate samples with the selected $Ce_{0.9}Tb_{0.1}O_2$ composition.[a].

Sample	Precursors (+additives)	Preparation conditions
COCl[a]COCl-W	$CeCl_3{\cdot}7H_2O$ (99.9%, Aldrich) $TbCl_3{\cdot}6H_2O$ (99.9%, Strem) (+NH_4OH)	Classical coprecipitation through NH_4OH addition (up to pH *ca.* 9), with subsequent washing (*COCl-W*) or without washing (*COCl*)
COCl-HT	$CeCl_3{\cdot}7H_2O$ (99.9%, Aldrich) $TbCl_3{\cdot}6H_2O$ (99.9%, Strem) (+NH_4OH)	Classical coprecipitation through NH_4OH addition (up to pH *ca.* 9), followed by hydrothermal treatment of colloidal solution in Teflon-sealed autoclave (250 °C/35 bar/18 h)
EV-NO3	$Ce(NO_3)_3{\cdot}6H_2O$ (99.9%, Strem) $Tb(NO_3)_3{\cdot}6H_2O$ (99.9%, Strem)	Simple evaporation method (100 °C/air) from initial nitrates solution (pH *ca.* 4–5)
CONO3-1	$Ce(NO_3)_3{\cdot}6H_2O$ (99.9%, Strem) $Tb(NO_3)_3{\cdot}6H_2O$ (99.9%, Strem) (+NH_4OH)	Classical coprecipitation through NH_4OH addition (up to pH *ca.* 9), without washing
CONO3-2	$Ce(NO_3)_3{\cdot}6H_2O$ (99.9%, Strem) $Tb(NO_3)_3{\cdot}6H_2O$ (99.9%, Strem) (+$NH_4OH + HNO_3$)	Classical coprecipitation through NH_4OH addition (pH *ca.* 9–10), followed by colloid stabilization with HNO_3 addition up to pH∼3.3
COOX	$Ce(NO_3)_3{\cdot}6H_2O$ (99.9%, Strem) $Tb(NO_3)_3{\cdot}6H_2O$ (99.9%, Strem) (+$C_2H_2O_4 + NH_4OH$)	Addition of oxalyc acid (ratio C_2H_2O4:Ce + Tb = 1.5:1) to nitrates solution, followed by oxalate coprecipitation with NH_4OH (up to pH *ca.* 9)
COUR-1	$Ce(NO_3)_3{\cdot}6H_2O$ (99.9%, Strem) $Tb(NO_3)_3{\cdot}6H_2O$ (99.9%, Strem) (+urea, 98.5%, Panreac)	Addition of urea to nitrates solution (molar ratio *urea:Ce + Tb* = 1.3:1) and homogeneous precipitation (upon heating) by urea hydrolysis
COUR-2	$Ce(NO_3)_3{\cdot}6H_2O$ (99.9%, Strem) $Tb(NO_3)_3{\cdot}6H_2O$ (99.9%, Strem) (+urea, 98.5%, Panreac)	As with COUR-1, but with molar ratio *urea:Ce + Tb* = 6:1
MW-UR1	$Ce(NO_3)_3{\cdot}6H_2O$ (99.9%, Strem) $Tb(NO_3)_3{\cdot}6H_2O$ (99.9%, Strem) (+urea, 98.5%, Panreac)	Homogeneous precipitation by urea hydrolysis (ratio *urea:Ce + Tb* = 1.3:1) in a Teflon-sealed (25 mL) reactor under microwave irradiation (W900/1 min, repeated three times)
SON-UR1	$Ce(NO_3)_3{\cdot}6H_2O$ (99.9%, Strem) $Tb(NO_3)_3{\cdot}6H_2O$ (99.9%, Strem) (+urea, 98.5%, Panreac)	Homogeneous precipitation (70 °C) by urea hydrolysis (ratio *urea:Ce + Tb* = 1.3:1), assisted with ultrasonic irradiation

[a] $Ce_{0.9}Tb_{0.05}Y_{0.05}O_2$ composition was also prepared in the preliminary study (using $YCl_3{\cdot}6H_2O$ as Y precursor, 99.9%, from Strem) along with other coprecipitate samples with chlorides (COCl) with compositions $Ce_{1-x}Tb_xO_2$ (x = 0.1, 0.2 and 0.3).

Leyca electron microscope (as grain mounts following conventional preparation and imaging techniques). The composition and chemical homogeneity of the samples (distribution of Tb/(Ce + Tb) ratio) was determined by semi-quantitative elemental analysis with an EDX analyzer (supplied by Oxford University) attached to the microscope.

In order to test the performance of the obtained CeO_2-Tb solid solutions as red ceramic pigments, the powders calcined at different temperatures were 5 wt% enamelled with a commercial double-firing transparent glaze (approximate Seger formula: SiO_2 = 6.916, Al_2O_3 = 0.633, K_2O = 0.094, Na_2O = 0.576, CaO = 0.193 and PbO = 0.137) onto conventional (fired) ceramic biscuits, and fired following a fast-firing scheme (52 min of duration from cool to cool at a maximum temperature of 1050 °C). The use of single-firing ceramic glazes of higher melting temperature (1050–1120 °C) was discarded to avoid degasification problems. Indeed, previous studies of G. Monrós et al. using these glazes confirm that the oxygen evolved (around 0.1–0.3 wt%, between 600 and 1100 °C) by CeO_2 reductive decomposition ($CeO_2 \rightarrow CeO_{2-x} + x/2\ O_2$) may remain occluded in the high-viscous melt and originate defects ("pin-hole" effect) on enamel surface,[55] as it also occurs with some Co-based pigments.[56] The optical properties of enamelled samples were analyzed by diffuse reflectance spectroscopy (VIS region) performed with a PerkinElmer (lambda 2000) spectrophotometer. In addition, $L^*/a^*/b^*$ colour parameters of enamelled samples were measured using a standard lighting C, following the CIE-$L^*/a^*/b^*$ colorimetric method recommended by the CIE (Commission Internationale de l'Eclairage).[57] On this method, L^* is the lightness axis (black (0) → white (100)), b^* is the blue (−) → yellow (+) axis, and a^* is the green (−) → red (+) axis.

3. Preliminary optimization of composition

In a preliminary study we analyzed the effect of Tb doping (and Y doping in samples with x = 0.05), and also the effect of using H_3BO_3 as mineralizer, on the formation and colouring performance of Tb-CeO_2 solid solutions. In this study, the optimal composition giving the best red colour was selected in samples prepared by the ceramic route and also through the conventional coprecipitation route (using chlorides as precursors).

3.1. XRD characterization and effect of H_3BO_3 mineralization

As the first important result, the XRD patterns of samples calcined at 1100 °C (see Fig. 1) indicate that Tb-doped ceria phases (C = CeO_2-Tb) form at lower temperatures through the use of the classical coprecipitation route (*COCl*), rather than by the conventional ceramic method (*CE*). Effectively, the corresponding XRD patterns of ceramic samples at 1100 °C still present peaks of residual Tb_4O_7 (T), non-integrated in the solid solution. In comparison, these Tb_4O_7 peaks are absent in coprecipitate samples for all compositions (even at x = 0.3). Moreover, in *COCl* samples the formation of ceria phase free of residual Tb_4O_7 and with an acceptable level of crystallinity was observed to take place at much lower temperatures, such as 600 °C (not shown).

As another important observation (see Fig. 1), in COCl samples the peaks associated to ceria solid solution (C) become slightly broader when increasing Tb doping (from x = 0.05–0.3), indicating a lower homogeneity of the formed solid solution the higher the Tb content (for x > 0.1). To determine whether different solid solutions were formed instead of a single solid solution, more precise and refined XRD patterns of coprecip-

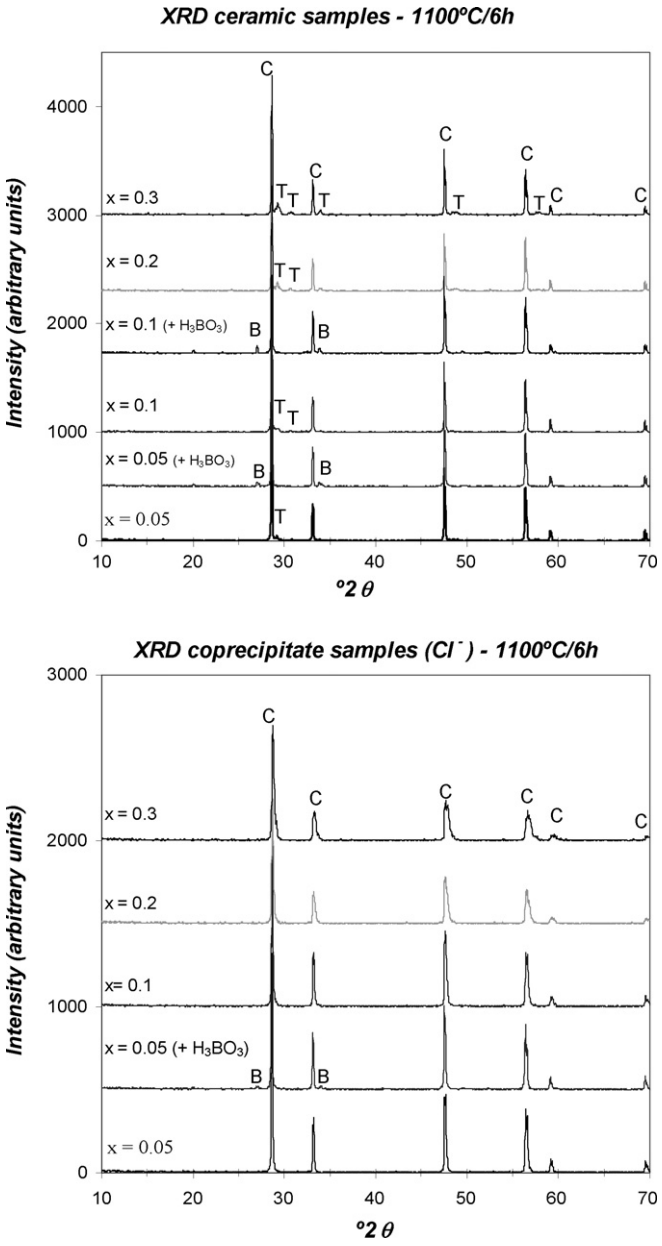

Fig. 1. XRD patterns of ceramic (above) and coprecipitate (below) $Ce_{1-x}Tb_xO_2$ ($x = 0.1$, 0.2 and 0.3) and $Ce_{0.9}Tb_{0.05}Y_{0.05}O_2$ (x = 0.05) samples fired at 1100 °C/6 h (C = CeO_2, T = Tb_4O_7 and B = borate phase). (For interpretation of the references to colour in this figure legend, the reader is referred to the web version of this article.)

itate samples fired at 1100 °C were obtained (not shown for brevity reasons). These patterns evidenced that a single phase of ceria was only obtained for $x = 0.05$ composition, doped with Y and Tb ($Ce_{0.9}Tb_{0.05}Y_{0.05}O_2$). For higher amounts of Tb doping ($x \geq 0.1$), however, the XRD peaks were splitted due to the presence of two different solid solutions, with different Tb content and cell parameters. From these refined XRD patterns at 1100 °C, the cell parameters of the different solid solutions were measured (see Table 2) in representative compositions. In sample with Tb and Y doping ($x = 0.05$) the single solid solution possesses a higher cell parameter (a value) of 5.41 Å, similar to that of non-doped ceria with fluorite-based structure ($a = 5.41$ Å for CeO_2, JCPDS 43-1002). This could be explained by the entrance of the smaller Tb^{4+} (1.02 Å) being compensated by the entrance of the larger Y^{3+} (1.16 Å), both in eightfold coordination, substituting for Ce^{4+} (1.11 Å). For higher amounts of Tb doping ($x = 0.1$–0.3) a first solid solution (C-1) with an almost similar cell parameter is also detected (a parameter of *ca.* 5.41 Å), but it is accompanied by a second solid solution (C-2) presumably more Tb^{4+}-enriched and having considerably smaller cell parameters (5.39 and 5.38 for $x = 0.1$ and 0.2, respectively; not measured for $x = 0.3$).

In the case of ceramic samples, however, the formation of ceria solid solutions free of residual Tb_4O_7 was only observed after calcination up to 1500 °C/1 h. After this firing treatment at 1500 °C, the XRD peaks of both coprecipitate and ceramic samples (not shown) are much narrower, suggesting the formation of a more homogeneous and better crystallized ceria solid solution. However, a more thorough analysis through refined XRD patterns indicated also in this case the formation of a single solid solution only for $x = 0.05$ and 0.1 in the case of COCl samples, and up to $x = 0.2$ for ceramic samples. Interestingly, the cell parameters (Table 2) were slightly smaller for COCl samples (5.40 Å for $x = 0.1$ and 5.38–5.41 Å for $x = 0.3$) than for ceramic samples (5.41 for $x = 0.1$ and 0.2), resulting in a slight shift of the XRD peaks to higher degrees of 2θ for the former (see a comparison in Fig. 2 for $x = 0.1$).

As for the use of H_3BO_3 as mineralizer, an interesting effect was also observed. As may be appreciated in Fig. 1, in ceramic compositions the addition of H_3BO_3 as mineralizer did not result in an improvement of ceria crystallization. On the contrary, an additional metallic borate phase crystallized (non-completely assigned, marked as *B* in XRD patterns and with main peaks at around 27 and 34°2θ) and became stabilized at 1100 °C in both

Table 2
Evolution of cell parameter (a) with composition and thermal treatment in representative $Ce_{1-x}Tb_xO_{2-y}$ coprecipitates (*COCl*) and ceramic samples (*CE*).

Lattice parameter (a, Å)[a]	$x = 0.05$[b] (+H_3BO_3)	$x = 0.10$[c]	$x = 0.20$[c]	$x = 0.30$[c]
COCl-1100/6 h	5.4112 (2)	C-1: 5.4069 (2) C-2: 5.3907 (5)	C-1: 5.4096 (3) C-2: 5.3768 (6)	Two phases (not measured)
COCl-1500/1 h	Not measured	5.4053 (1)	Two phases (not measured)	C-1: 5.4061 (6) C-2: 5.3833 (2)
CE-1500/1 h	Melted	5.4116 (1)	5.4107 (2)	Two phases (not measured)

[a] $a = 5.41134$ Å for non-doped ceria (CeO_2, JCPDS 43-1002).
[b] Composition $Ce_{0.9}Tb_{0.05}Y_{0.05}O_{2-y}$ with H_3BO_3 (2 wt%) mineralization.
[c] The formation of an homogeneous single phase was not achieved in some samples, the XRD patterns indicating the coexistence of two different cerianite phases, denoted as C-1 and C-2 (solid solutions with different Tb^{4+} content, and thus with different lattice parameters).

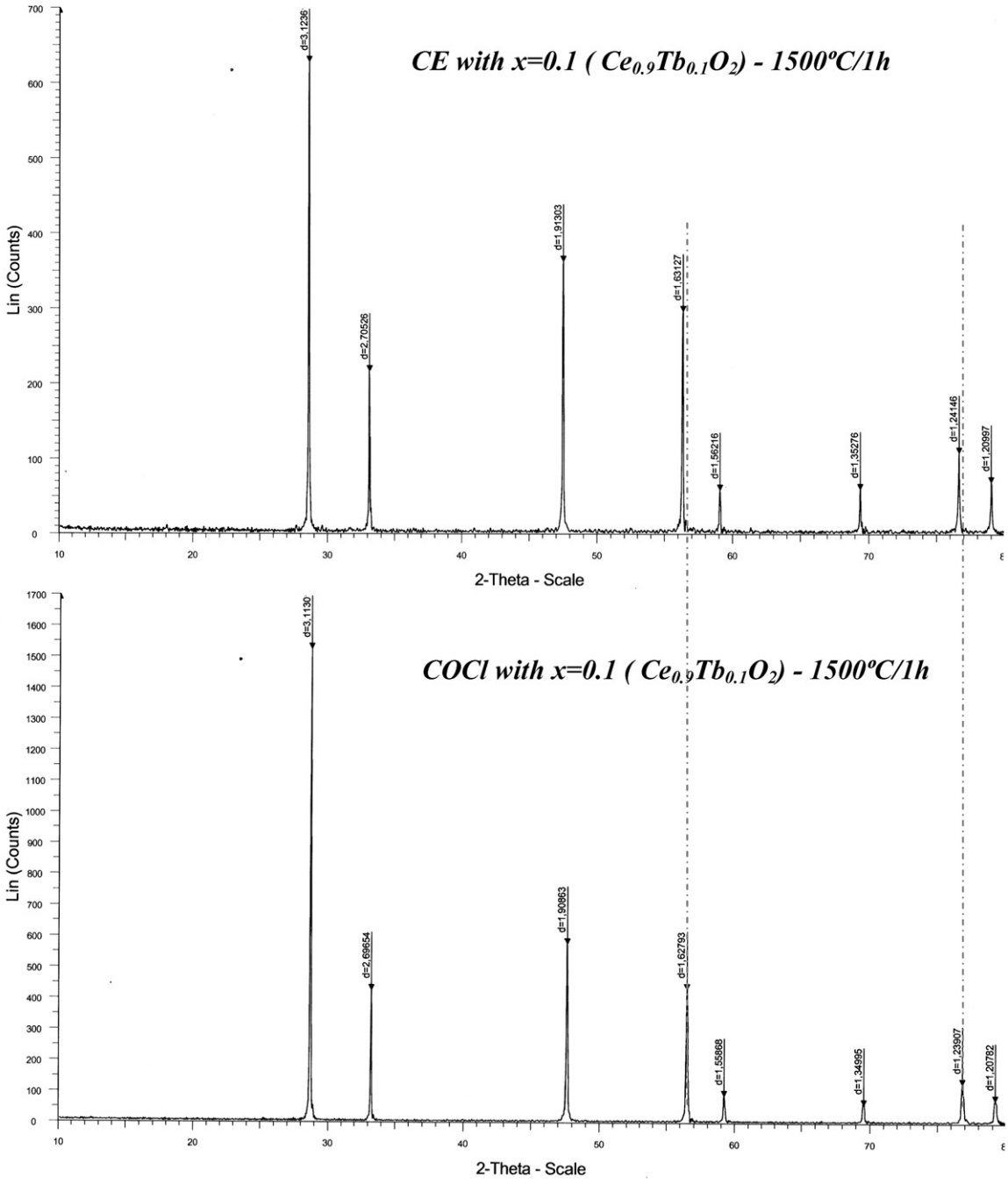

Fig. 2. Refined XRD patterns (step = 0.02°2θ, t = 3 s) of ceramic (*CE*, above) and coprecipitate (*COCl*, below) samples with composition $Ce_{0.9}Tb_{0.1}O_2$ (x = 0.1) fired at 1500 °C/1 h. In both cases a single phase of cerianite (C) is observed (a = 5.405 Å for *COCl* and a = 5.412 Å for *CE*).

compositions (x = 0.05 and 0.1). The stabilization of this phase is also observed in coprecipitate sample (x = 0.05) at 1100 and 1300 °C (not shown). However, this phase is absent at 1500 °C and it is still not formed at 600 °C (not shown). This metal borate must presumably contain some amount of Tb, considering the much poorer red colour of these compositions at these temperatures (later commented). The fact, that residual Tb_4O_7 peaks are detected in the non-mineralized composition with x = 0.1, but Tb_4O_7 is not present in the mineralized sample (Tb could be then incorporated in the metal borate phase), is also in agreement with this hypothesis.

3.2. Microstructure and composition characterization

Representative SEM details (obtained with backscattering electron detector) of ceramic and coprecipitate samples (for x = 0.1) are shown in Fig. 3. As it may be appreciated, ceramic samples (CE) after calcination are constituted by large particles forming aggregates *ca.* 10–80 (m-sized, while coprecipitates (COCl) consist of nanostructured morphologies (round-shaped grains *ca.* 100–300 nm). On the other hand, the corresponding EDX analyses showed a sufficiently homogeneous distribution (at the microscale) of Tb throughout coprecipitate samples (nar-

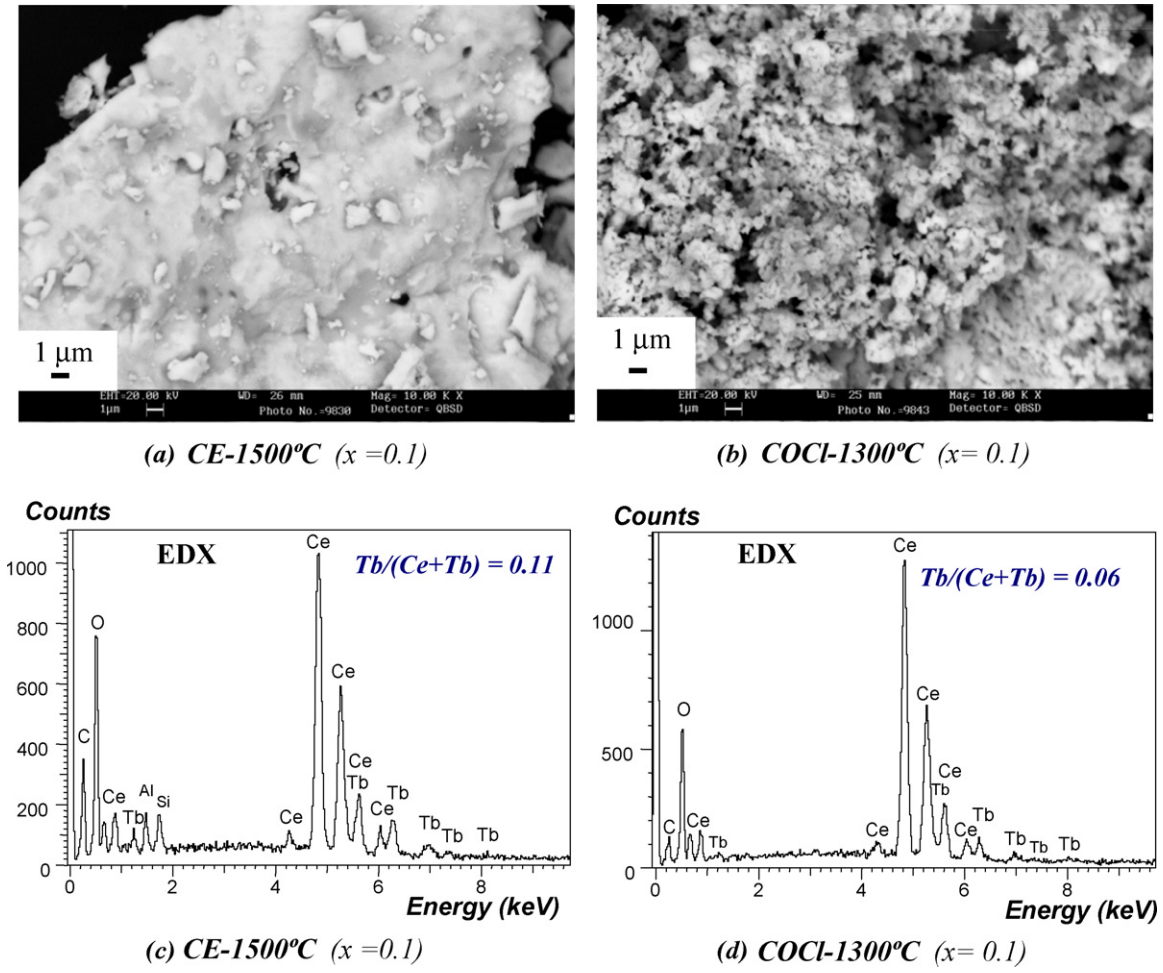

Fig. 3. Representative SEM images of fired samples with composition $x = 0.1$ ($Ce_{0.9}Tb_{0.1}O_2$): (a) ceramic sample fired at 1500 °C/1 h and (b) coprecipitate (COCl) sample fired at 1300 °C/1 h. The corresponding EDX spectra are shown in (c) and (d), respectively.

row dispersion of the values of Tb/(Ce + Tb) ratio). Average values for this ratio are given for representative samples in Table 3 (along with the measured colour parameters). Noteworthy, the measured average composition was close to the theoretical (initial) formulation in ceramic samples, while a significant stoichiometric loss of Tb was detected in coprecipitate samples (presumably due to insufficient precipitation from the liquid phase), except in mineralized composition ($x = 0.05$, with 2 wt% addition of H_3BO_3). As previously commented, addition of H_3BO_3 as mineralizer does not result in an enhancement of the crystallization rate of Tb-CeO_2 solid solution, but it could allow to reduce significantly the loss of Tb due to the stabilization of a Tb-containing borate phase (detected as crystalline phase at temperatures above 600 °C and below 1500 °C).

3.3. Colour performance as red ceramic pigments and selection of optimal composition

With the entrance of Tb^{4+} in ceria (CeO_2) lattice, the absorption band in the indigo region (with light yellow as complementary observed colour) is shifted to higher wavelengths

Table 3
Evolution of colorimetric parameters ($L^*/a^*/b^*$) with composition and thermal treatment in $Ce_{1-x}Tb_xO_{2-y}$ coprecipitates (*COCl*) and ceramic samples (*CE*). Average EDX values for Tb/(Ce + Tb) are given in some cases (between brackets).

$L^*/a^*/b^*$ (Tb/(Ce + Tb)EDX)[a]	$x = 0.05$[b]	$x = 0.05$[b] (+H_3BO_3)	$x = 0.10$	$x = 0.20$	$x = 0.30$
COCl-1100/6 h	73.6/13.1/25.0	76.7/6.7/23.2	71.1/13.4/26.3	67.0/14.0/27.5	66.8/13.7/26.5
COCl-1300/1 h	68.9/13.9/25.4 (0.024)	71.1/13.6/30.9 (0.047)	66.2/15.7/28.9 (0.061)	62.7/14.9/26.6 (0.134)	63.5/13.9/27.0 (–)
COCl-1500/1 h	62.9/21.1/32.5	58.9/23.8/32.5	59.0/21.0/30.8	53.9/17.4/24.3	52.5/15.7/22.2
CE-1500/1 h	64.5/22.0/33.6 (0.047)	Melted	60.7/24.5/33.9 (0.112)	58.4/23.5/31.3 (0.187)	61.6/19.1/32.2 (–)

[a] The average values of Tb/(Ce + Tb) ratio (experimental x values) obtained by EDX for representative compositions are indicated between brackets (CO-1300 and CE-1500 samples).

[b] Composition $Ce_{0.9}Tb_{0.05}Y_{0.05}O_{2-y}$ without or with H_3BO_3 (2 wt%) mineralization.

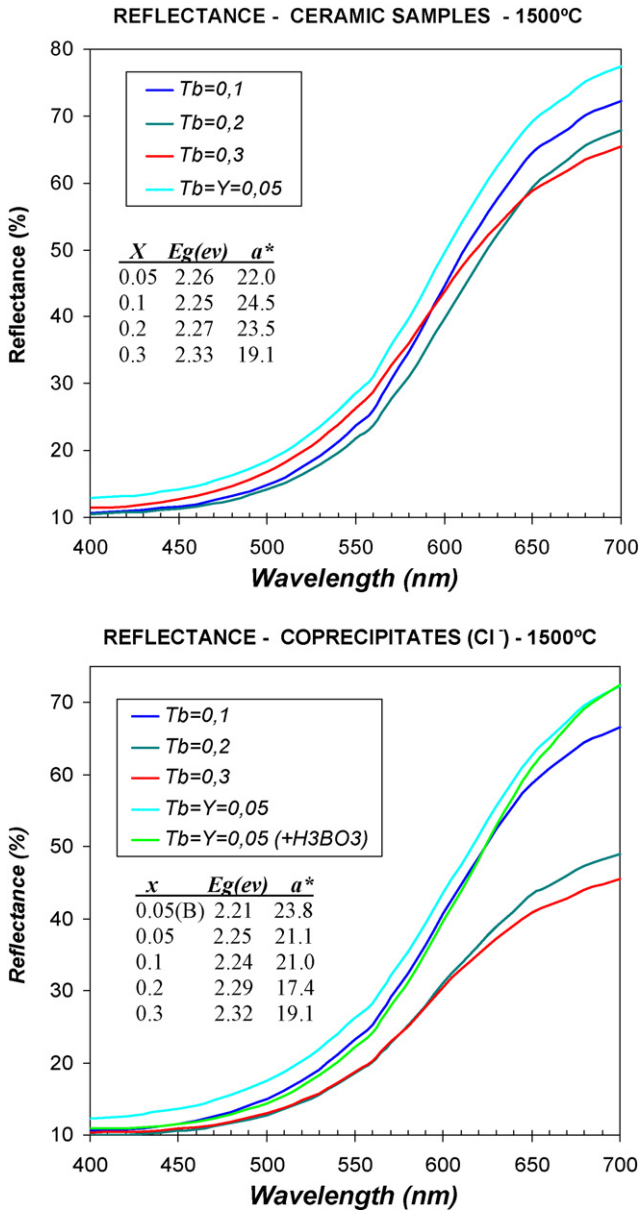

Fig. 4. Reflectance curves of enamelled samples with $Ce_{1-x}Tb_xO_2$ ($x = 0.1$, 0.2 and 0.3) and $Ce_{0.9}Tb_{0.05}Y_{0.05}O_2$ ($x = 0.05$) pigments fired at 1500 °C/1 h. Ceramic samples above and coprecipitates below. The values of the bandgap (E_g) are also given, showing its correlation with reddish colour (a^*). (For interpretation of the references to colour in this figure legend, the reader is referred to the web version of this article.)

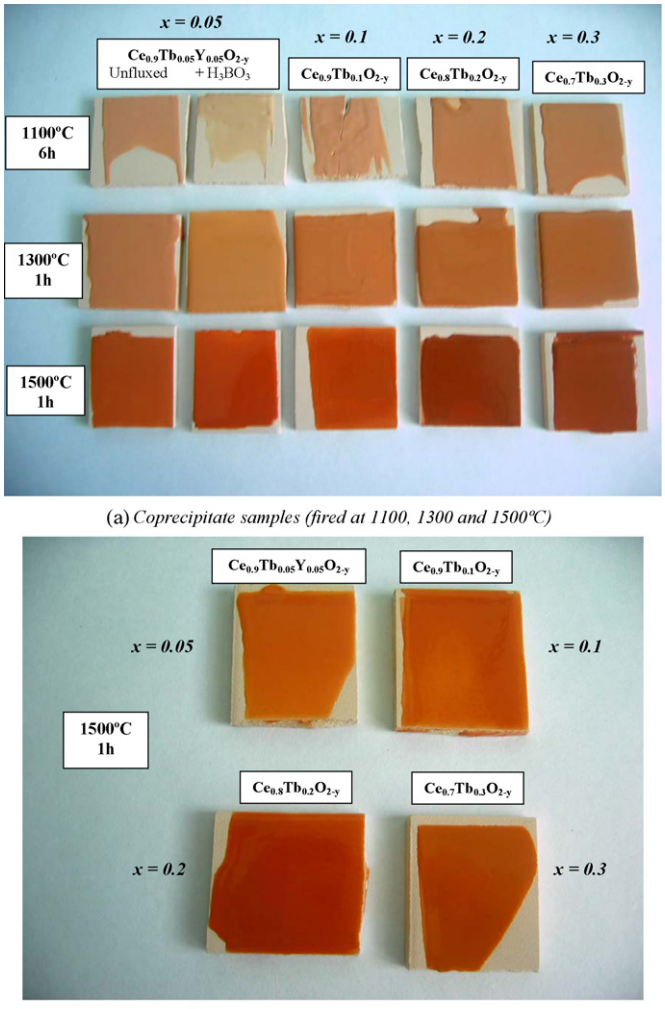

Fig. 5. Aspect of coprecipitate (above) and ceramic samples (below; 1500 °C) once enamelled with a double-firing ceramic glaze (5 wt% of pigment) onto conventional ceramic tiles. Ceramic samples where white-coloured below 1500 °C (not shown). (For interpretation of the references to colour in this figure legend, the reader is referred to the web version of this article.)

(around 460–480 nm). Thus, the bandgap threshold associated to non-doped ceria (2.76 eV) becomes reduced to lower values (lower energies), giving rise to reddish colourations.[21,43] Accordingly, incorporation of Tb in ceria solid solution should result in a minimum reflectance around 460–500 nm (due to the complementary absorption band around 460–480 nm), and a maximum reflectance centred in the red region (at *ca.* 650–700 nm).

Effectively, diffuse reflectance spectra of enamelled samples (see spectra of 1500 °C-calcined samples in Fig. 4) having the best red colours ($x \leq 0.1$) present a much more marked maximum reflectance between 600 and 700 nm (and a rather similar minimum reflectance between 400 and 550 nm). From these reflectance curves the bandgap (E_g) wavelengths or energies were also calculated. The values of E_g (also shown in Fig. 4) confirm that the poorer red compositions posses higher energy bandgap (E_g) values (2.27–2.33 eV), and correspond to higher doped compositions ($x > 0.1$). In comparison, compositions with $x \leq 0.1$ posses lower energy E_g values around 2.21–2.25 (eV) and better red colourations.

Also regarding to the colour of the fired pigments (see the aspect of enamelled samples in Fig. 5), coprecipitate samples developed reddish colourations at much lower temperatures (*i.e.* 1100 and 1300 °C) than ceramic ones, in agreement with the earlier formation of ceria solid solutions in the former. Taking into account the measured colour parameters of enamelled samples (L^*/a^*b^* values are also shown in Table 3), the red colour of *COCl* samples improves (higher a^* value) with increasing firing temperature from 1100 to 1500 °C, due to a better development of Tb-doped ceria solid solution. Ceramic compositions

were still white-coloured after firing treatments at 1100 °C/6 h or 1300 °C/1 h, and for this reason they were not enamelled at these temperatures.

As it may be appreciated the composition at 1500 °C having the best red colour (higher a^* and lower b^* and L^* values) is $Ce_{0.9}Tb_{0.1}O_{1.95}$ ($x = 0.1$) both in *CE* and *COCl* samples (for instance, $a^* = 24.5$ for *CE* sample). Coprecipitate samples with $x = 0.05$ and 0.1 have slightly lower red hues (a^* *ca.* 21) than ceramic composition, although they have also a slightly higher intensity (related with its lower L^* value) and a lower yellow component (lower b^*). Noteworthy, Tb and Y-doped coprecipitate composition with $x = 0.05$ ($Ce_{0.9}Tb_{0.05}Y_{0.05}O_2$) and with H_3BO_3 mineralization yields even a better red colour (a^* *ca.* 24) than composition with $x = 0.1$ (the corresponding ceramic sample melted at this temperature), but at lower temperatures the red colour is much poorer. The lower red colour of this composition at 1100 ($a^* = 6.7$) and 1300 °C ($a^* = 13.6$) could be presumably due to the stabilization of a metallic borate (*B*) phase containing Tb and/or cerium, as it was previously commented, and for this reason this composition was not selected for the following study. Thus, and according to the colour performance of both ceramic and coprecipitate samples, the selected composition giving the optimal reddish colouration was $Ce_{0.9}Tb_{0.1}O_{1.95}$ (with $x = 0.1$).

4. Effect of synthesis methods on solid solution formation and colouring performance

The second main objective of this work was to optimize the colour of Tb-doped compositions at lower temperatures through the use of non-conventional synthesis routes. As we showed in previous section, ceria-based pigments obtained at 1100 °C with the classical coprecipitation method (with chlorides) still have considerably poorer reddish colourations (a^* value between 13 and 14) than the ceramic compositions calcined at 1500 °C (a^* values around 22–24.5). In this section we demonstrate the possibility of improving a great deal the red colour of Tb-doped ceria pigments (having the selected optimal composition, $x = 0.1$) at 1100 °C or even lower temperatures, through the use of other non-conventional coprecipitation routes.

4.1. Thermal analysis

Thermal analyses were performed with all the prepared samples (representative DTA-TG curves are shown in Fig. 6). According to these analyses, the decomposition or elimination processes (H_2O, Cl^-, NO_3^-, NH_3, ...) with the corresponding weight loss (and endothermic peaks) are observed to take place below 300 °C for nitrates samples and below 400–450 °C for

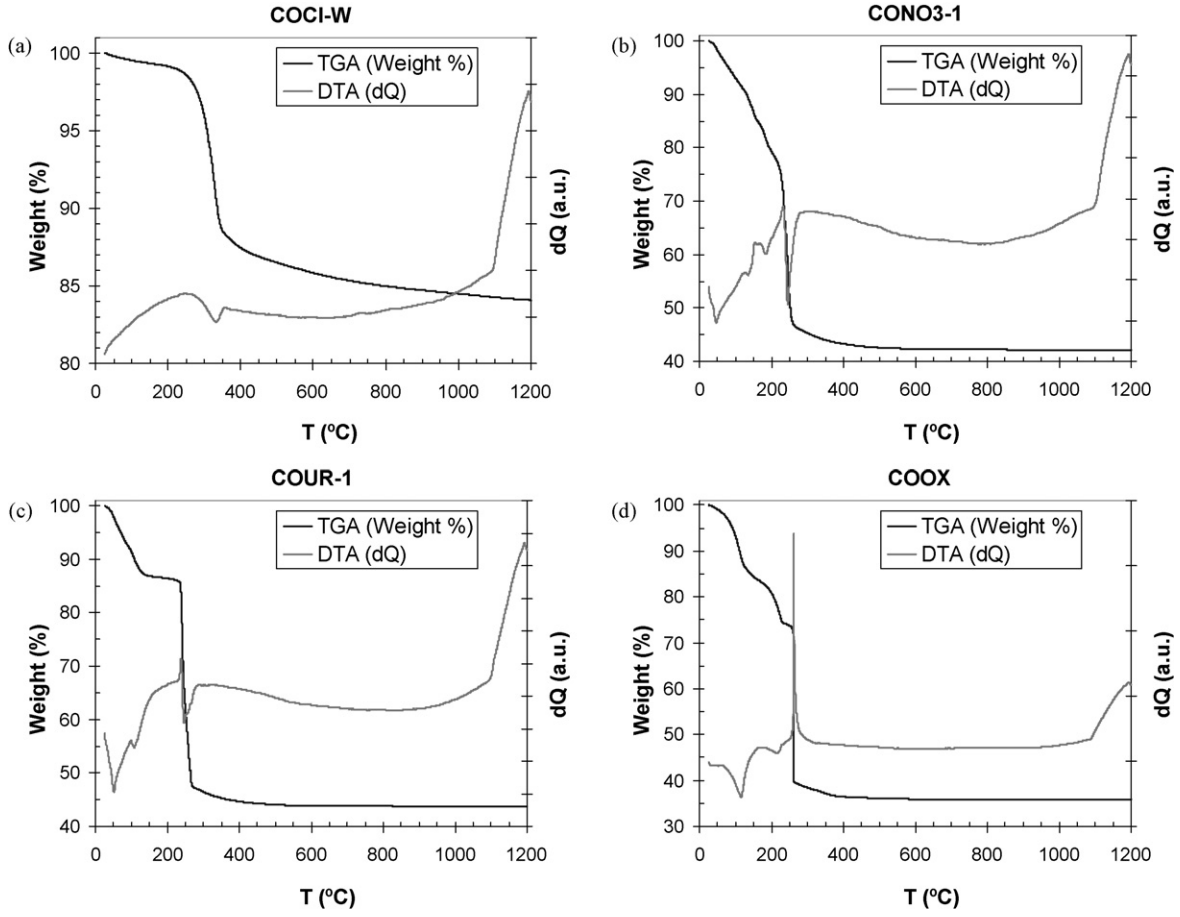

Fig. 6. Thermogravimetric (TGA) and differential thermal analysis (DTA) of representative *coprecipitate* samples: (a) *COCl-W*, (b) *CONO3-1*, (c) *COUR-1* and (d) *COOX*.

chlorides samples. In samples containing organics (for instance, in the case of COOX sample), a sharp and intense exothermic peak due to organics decomposition is observed in the DTA curve at around 260 °C. Noteworthy, in samples with chlorides as precursors there is also an important and steady weight loss at higher temperatures (600–1100 °C), non-observed in nitrates samples. This could suggest that some chlorides are still removed at these higher temperatures, but the associated slight and continuous exothermic increase in the DTA curve observed from these temperatures (from 600 °C in chlorides samples against 800 °C or even higher temperatures for nitrates samples) could be also associated to the reductive decomposition of CeO_2 to CeO_{2-x} (with the corresponding O_2 evolution). In all samples, this decomposition is much more enhanced at higher temperatures (from 1100 °C), being responsible for the clear and intense exothermic peak at these temperatures. This reductive process is quite important and should be avoided as much as possible, since this could originate the classical "pin-hole" defect when enamelling the pigment with ceramic frits possessing higher melting temperatures (single-firing or porcelainized glazes, which melt above 1100 °C).[55]

4.2. XRD characterization: evolution of cerianite crystallization and lattice parameters

The observation of XRD patterns of samples fired at 400 °C (see Fig. 7) evidences an incipient crystallization of CeO_2-Tb solution at such low temperatures, without the presence of any residual phase of terbium oxide. In *classical coprecipitation* samples (above), this crystallization is clearly more advanced in chlorides samples than in nitrates samples. As it was to be expected, *COCl-HT* sample presents the most grown cerianite crystals, since this sample was previously hydrothermally treated at 250 °C. On the other hand, in the case of *homogeneous coprecipitation* samples fired at 400 °C (below), the crystallization is also less intense than in chlorides samples, except in urea sample *COUR-2*. As it may be clearly appreciated (Fig. 7) in urea coprecipitates, the increase of the ratio *urea:metal* from 1.3:1 (*COUR-1* sample) to 6:1 (*COUR-2* sample) results in a much more advanced crystallization of cerianite in the later.

As for the samples calcined at 1100 °C (Fig. 8, above), in *classical coprecipitation* routes the crystallization of CeO_2-Tb solid solution is very similar, although slightly more intense with chlorides than with nitrates samples (and especially in hydrothermal sample, *COCl-HT*). In contrast, in *homogeneous coprecipitation* samples (Fig. 8, below) important differences may be observed. In urea coprecipitates an inversion occurred in comparison with 400 °C-calcined samples. Indeed, although sample *COUR-1* showed at 400 °C a less intense crystallization, it is this sample the one with the most advanced crystallization at 1100 °C. Besides, sample *MW-UR1* obtained with microwaves assistance presents a similar (advanced) crystallization than COUR-1. On the contrary, coprecipitate sample assisted with ultrasounds (*SON-UR1*) appears to be very poorly crystallized at 1100 °C, similarly to oxalate coprecipitate sample (*COOX*). It must be highlighted that the precursor powder of *MW-UR1* sample was obtained in a very short reaction time (below 10 min), while the other samples involve several hours of reaction time before being submitted to the calcination treatment. This synthesis advantage has an important value from energy savings considerations or environmental concerns. The evolution with the firing temperature of the most intense XRD peak of cerianite phase may be also followed in Tables 4 and 5 (the intensity counts are given). Both tables summarize all the characterization results obtained with the studied coprecipitate samples, as it will be later discussed.

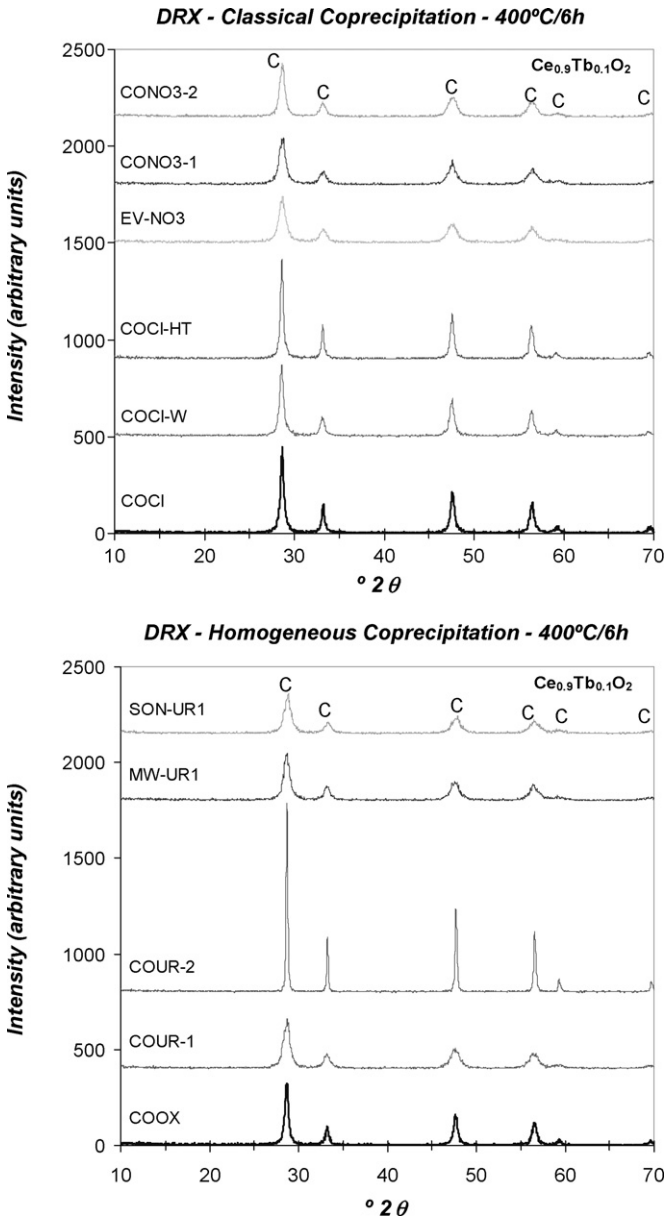

Fig. 7. XRD patterns of classical coprecipitation samples (above; including *hydrothermal* sample) and homogeneous coprecipitation samples (below) $Ce_{0.9}Tb_{0.1}O_2$ fired at 400 °C/6 h (C = CeO_2).

In order to confirm whether homogeneous solid solutions were formed or not, more refined XRD patterns of all samples were also obtained at 1100 °C, and with these patterns the cell parameters of the formed CeO_2-Tb solid solutions were esti-

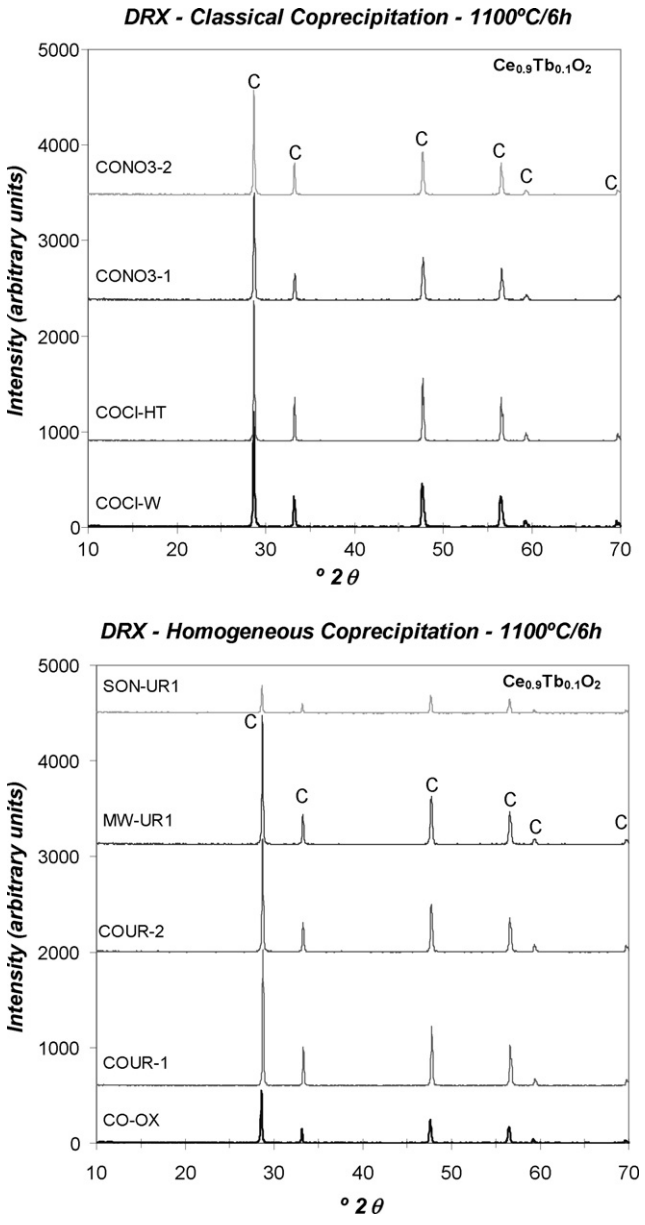

Fig. 8. XRD patterns of classical coprecipitation samples (above; including *hydrothermal* sample) and homogeneous coprecipitation samples (below) $Ce_{0.9}Tb_{0.1}O_2$ fired at 1100 °C/6 h (C = CeO_2).

mated (see results also in Tables 4 and 5). With these refined XRD patterns it was evident that some classical coprecipitate samples do not contain a single phase of cerianite (since each XRD peak appears splitted in two distinct peaks). Indeed samples COCl, EV-NO3 and CONO3-1 are the least homogeneous, containing all of them two distinct cerianite phases (Table 4): a first cerianite phase appearing at lower 2θ values (C-1 phase) and possessing larger cell parameters (*ca.* 5.41 Å), and a second cerianite phase appearing at higher 2θ values (C-2 phase) and possessing smaller cell parameters (*ca.* 5.39 Å). The other classical coprecipitates (COCl-W, COCl-HT and CONO3-2) are more homogeneous and contain only a single phase with an intermediate cell parameter of *ca.* 5.40 Å. In contrast, all homogenous coprecipitation samples are formed by a single phase of cerianite (Table 5), in agreement with the more homogenous precursors obtained with these synthesis methods. Noteworthy, homogeneous coprecipitation samples present all of them the same cell parameter of *ca.* 5.40 Å. This cell parameter value is only slightly smaller than the theoretical value for the non-doped cerianite lattice ($a = 5.41134$ Å for CeO_2, JCPDS card no. 43-1002). The entrance of the smaller Tb^{4+} ions (1.02 Å) in the fluorite lattice (eightfold coordination) replacing for Ce^{4+} ions (1.11 Å) would explain the smaller cell parameters. However, any interpretation of the variation of cell parameters in this system is not so simple, since some amount of the larger Ce^{3+} (1.28 Å) and Tb^{3+} (1.18 Å) ions are also very likely to be present[42] (accompanied by some oxygen vacancies to preserve electroneutrality), although the performance of further analyses to estimate their presence (*i.e.* by XANES spectroscopy) is out of the scope of this study.

4.3. Microstructure and composition (SEM/EDX) characterization

To gain further information about the morphology, homogeneity and composition of the samples at the microscale, SEM/EDX characterization was performed with representative fired samples. SEM observations of pigments calcined at 1100 °C (see Fig. 9 for classical coprecipitation, and Fig. 10 for homogeneous coprecipitation samples) let us appreciate that the samples are formed by aggregates constituted by submicronic particles or grains (100–300 nm) with rounded morphologies and also with intergranular porosity. In general terms, the morphology is quite homogeneous in those samples that were formed by a single phase of cerianite according to the previous XRD characterization (*COCl-W*, *COCl-HT*, *CONO3-2*). In contrast, sample CONO3-1 (see Fig. 9) presents a more hetereogeneous morphology, in accordance with the presence of two regions (solid solutions) with different Tb content as it will be later discussed.

The approximate average Tb content and homogeneity degree of the formed $Ce_{1-x}Tb_xO_2$ solid solutions could be qualitatively estimated through the measurement of $Tb/(Ce + Tb)$ molar ratios (x). With this aim, representative EDX analyses were performed in different regions of the samples. As it may be observed (Tables 4 and 5), in the case of classical coprecipitate samples the average Tb content (x value) was almost in all samples between 0.06 and 0.08 (Table 4), which is below the theoretical value of the initial formulation ($x = 0.10$). Differently, the average Tb content was considerably higher in *CONO3-2* sample ($x = 0.13$). This sample was prepared through the so called "colloid stabilization route", a modification of the classical coprecipitation route (sample *CONO3-1*) in which the growth of coprecipitated colloidal particles is controlled (inhibited) by decreasing the pH down to a value of *ca.* 3.3 with HNO_3 addition. Therefore, this modification of the pH of the initial precursor system could presumably have some effect in the precipitation of Tb and Ce during the synthesis step, resulting in a higher Tb content. Also remarkably, in general terms the measured Tb ratios were rather disperse in these classical coprecipitate samples, indicative of a lack of homogeneity in the distribution of Tb throughout the samples. In this respect, sample *CONO3-1* appears to be the

Table 4
Results of XRD, cell parameters, EDX analyses, colour ($L^*/a^*/b^*$) and bandgap (E_g) measurements (enamelled samples) in $Ce_{0.9}Tb_{0.1}O_2$ samples obtained through *classical coprecipitation methods*.

Sample method	Firing treatments	XRD[a]	Unit cell a (Å)	Tb/(Ce + Tb)$_{EDX}$[b]	$L^*/a^*/b^*$	E_g (eV)[d]
	400 °C/6 h	C (440)			78.3/8.0/22.2	
COCl	600 °C/6 h	C (710)				
	1100 °C/6 h	C (1200)[c]	5.3907 (5)/5.4069 (5)	0.06	71.1/13.4/26.3	2.39
	400 °C/6 h	C (370)			77.3/8.9/24.2	
COCl-W	600 °C/6 h	C (470)			76.9/9.3/24.2	
	1100 °C/6 h	C (1270)	5.3999 (2)	0.07	69.8/16.1/31.9	2.37
COCl-HT	400 °C/6 h	C (510)			75.0/9.7/24.4	
	600 °C/6 h	C (760)			72.9/11.7/28.2	
	1100 °C/6 h	C (1450)	5.3998 (0)	0.08	63.4/20.0/35.8	2.28
	400 °C/6 h	C (235)			73.5/12.5/29.6	
EV-NO3	600 °C/6 h	C (410)			73.6/13.0/29.7	
	1100 °C/6 h	C (990)[c]	5.3912 (6)/5.4102 (2)		60.2/20.8/33.1	2.27
	400 °C/6 h	C (240)			76.9/10.1/24.2	
CONO3-1	600 °C/6 h	C (370)			74.6/12.3/26.0	
	1100 °C/6 h	C (1120)[c]	5.3944 (3)/5.4083 (3)	0.08	65.9/16.5/28.4	2.32
	400 °C/6 h	C (275)			67.1/17.7/31.2	
CONO3-2	600 °C/6 h	C (370)			66.1/19.0/31.5	
	1100 °C/6 h	C (1080)	5.3988 (1)	0.13	53.1/24.8/29.5	2.21

[a] C = CeO_2 (cerianite; JCPDS card no. 43-1002; a = 5.41134 Å); the XRD intensity of the most intense diffraction peak of CeO_2 is indicated between brackets.
[b] Average molar ratio (x = Tb/(Ce + Tb)) by EDX analyses performed in different (representative) regions of the samples (in COCl it was at 1300 °C/1 h instead of 1100 °C/1 h).
[c] Two cubic phases of ceria (with different cell parameters) distinguished by refined XRD.
[d] Approximate bandgap values (E_g) in eV calculated from reflectance curves (Fig. 11).

most heterogeneous and this fact may be easily observed in the SEM image shown as example in Fig. 9, with regions having different morphology and brightness contrast (distinct composition). The corresponding EDX analyses also shown in the figure clearly indicate the presence of these Tb-enriched and Ce-enriched regions in the same aggregate, with rather different Tb/(Ce + Tb) ratios (x = 0.16 and 0.04, respectively).

In contrast, the morphology was more homogeneous (see Fig. 10) and also the distribution of Tb through the samples more regular (levelled) in samples obtained by homogeneous coprecipitation of oxalates or with urea. Interestingly, the average Tb content (see Table 5) in these samples was much more approximated (0.08–010) or similar to the theoretical formulation (x = 0.1). A representative EDX analysis corresponding

Table 5
Results of XRD, cell parameters, EDX analyses, colour ($L^*/a^*/b^*$) and bandgap (E_g) measurements (enameled samples) in $Ce_{0.9}Tb_{0.1}O_2$ samples obtained through *homogeneous coprecipitation methods*.

Sample method	Firing treatments	XRD[a]	Unit cell a (Å)	Tb/(Ce + Tb)EDX[b]	$L^*/a^*/b^*$	E_g (eV)[c]
	400 °C/6 h	C (320)			71.8/15.3/31.5	
COOX	600 °C/6 h	C (365)			71.6/15.2/31.6	
	1100 °C/6 h	C (550)	5.3976 (1)	0.10	59.0/21.6/30.6	2.30
	400 °C/6 h	C (260)			72.8/13.9/32.6	
COUR-1	600 °C/6 h	C (400)			71.7/14.8/32.6	
	1100 °C/6 h	C (1400)	5.3984 (2)	0.09	58.5/22.8/34.1	2.27
	400 °C/6 h	C (980)			71.8/16.2/35.1	
COUR-2	600 °C/6 h	C (840)			73.1/15.3/35.1	
	1100 °C/6 h	C (1180)	5.4000 (1)	0.08	64.6/20.8/34.3	2.30
	400 °C/6 h	C (245)			75.6/11.8/28.8	
MW-UR1	600 °C/6 h	C (430)			73.3/13.3/28.9	
	1100 °C/6 h	C (1340)	5.3991 (2)	0.10	64.5/18.9/30.3	2.31
	400 °C/6 h	C (210)			73.0/13.2/29.0	
SON-UR1	600 °C/6 h	C (240)			70.4/15.0/28.7	
	1100 °C/6 h	C (290)	5.3989 (1)	0.09	57.0/21.0/28.3	2.29

[a] C = CeO_2 (cerianite; JCPDS card no. 43-1002); the XRD intensity of the most intense diffraction peak of CeO_2 is indicated between brackets.
[b] Average molar ratio (x = Tb/(Ce + Tb)) by EDX analyses performed in different (representative) regions of the samples.
[c] Approximate bandgap values (E_g) in eV calculated from reflectance curves (Fig. 11).

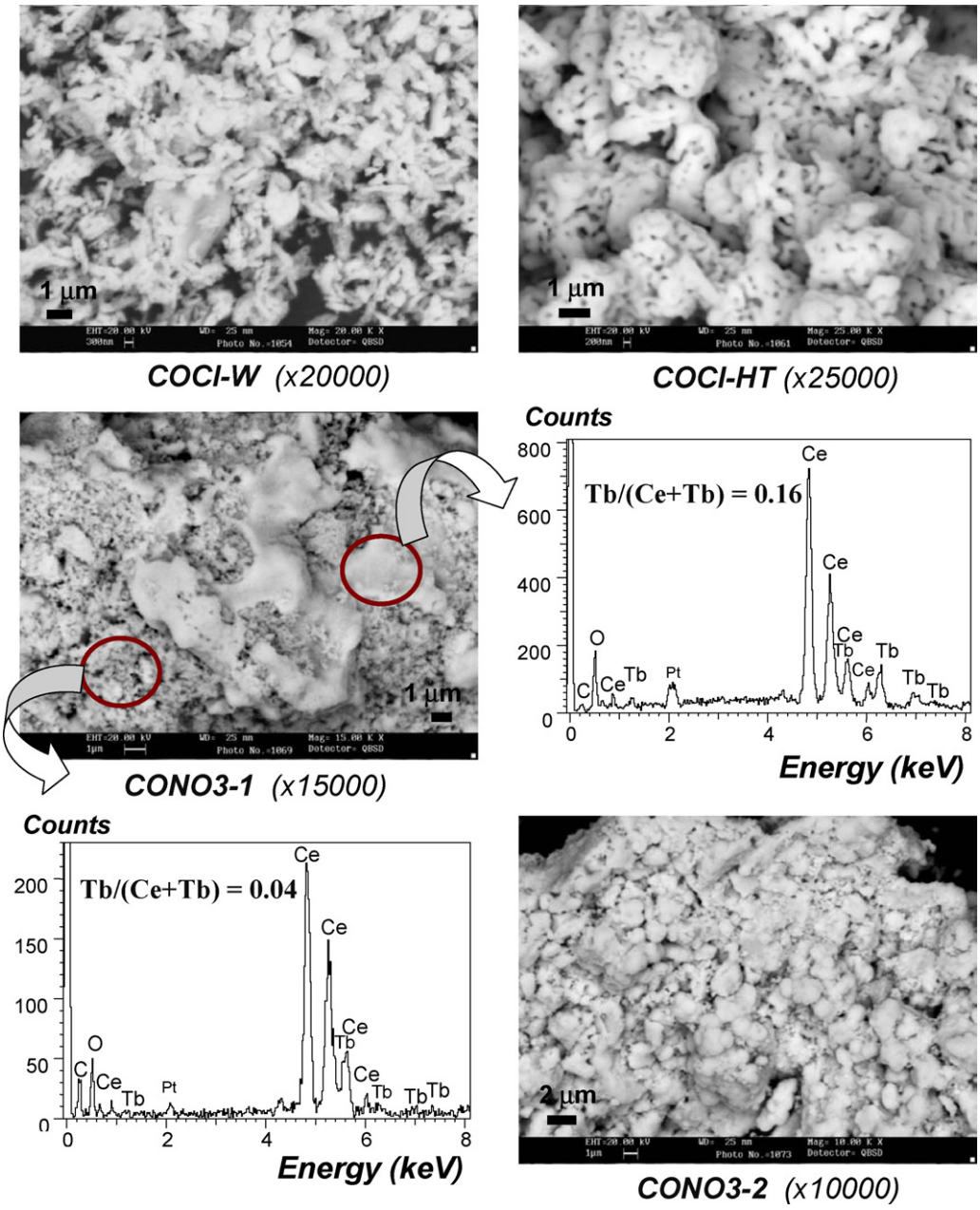

Fig. 9. Selected SEM details (back-scattered electron detector) of *classical coprecipitate samples* (COCl-W, COCl-HT, CONO3-1 and CONO3-2) calcined at 1100 °C/6 h. Two representative EDX spectra corresponding to *CONO3-1* sample (distinct marked areas) are also included. (For interpretation of the references to colour in this figure legend, the reader is referred to the web version of this article.)

to *COOX* sample is also shown in Fig. 10. Sample *COUR-2* presented the lower (average) Tb content ($x = 0.8$), while the distribution of Tb was less regular or homogeneous in microwave-assisted sample (*MW-UR1*), similarly to that of samples prepared by classical coprecipitation.

4.4. Comparative analysis of colour performance as red ceramic pigments

As the final part of the study we analyzed the colour performance of the prepared CeO_2-Tb pigments at different firing temperatures. The evolution of colour parameters ($L^*/a^*/b^*$) with different firing temperatures is also presented in Tables 4 and 5, while the aspect of all enamelled samples may be appreciated in the photos shown in Fig. 11. As the first important result, in some synthesis methods (*CONO3-2*, *COUR-2* and *COOX*) it was possible to develop acceptably nice red colours ($a^* = 15$–18), even after calcination at a temperature as low as 400 °C (the best colouration at this temperature being for *CONO3-2* sample, $a^* = 18$).

Taking into consideration the colours developed by 1100 °C-fired pigments, the results indicate that there is no direct correlation between the level of ceria crystallization (intensity of XRD peaks) and the reddish tonality (improves with higher a^* and lower b^* and L^* values). For example, coprecipitate samples with chlorides precursors (except hydrothermal sample) pro-

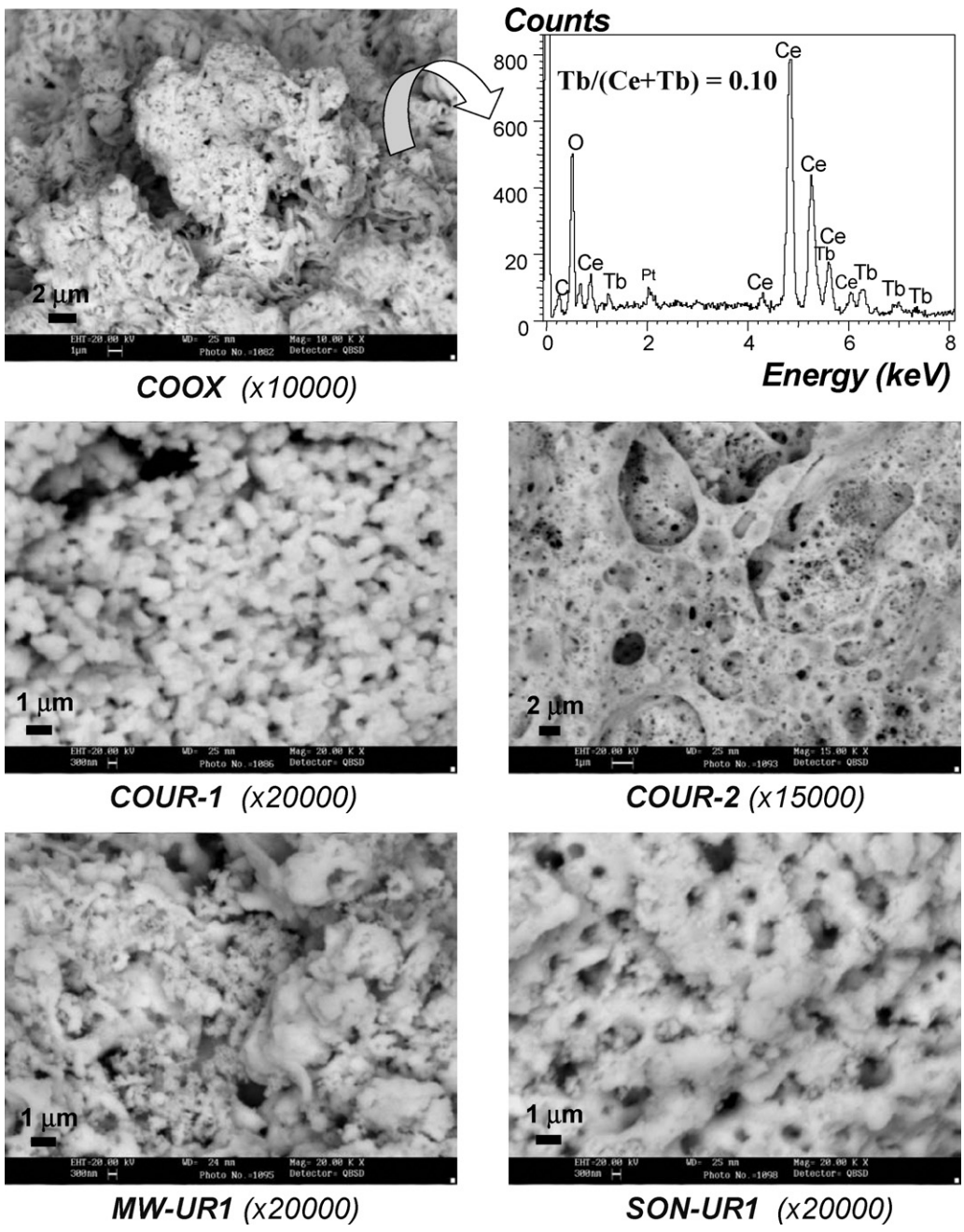

Fig. 10. Selected SEM details (back-scattered electron detector) of *homogeneous coprecipitate samples* (COOX, COUR-1, COUR-2, MW-UR1 and SON-UR1) calcined at 1100 °C/6 h. A representative EDX analysis (of COOX sample) is also included.

duce the worst red–orange colours ($a^* = 13$–16), though having a good crystallization degree of Tb-CeO_2 solid solution. In contrast, the very poorly crystallized samples with oxalates (*COOX*) or with urea and ultrasounds (*SON-UR1*) exhibit however very good red colours ($a^* = 21$–22).

On the contrary, the best red colours seem to be associated in first term to a higher Tb content, with the exception of microwave sample (which possessed a non-regular Tb distribution). In this respect, *CONO3-2* presents a much more reddish colouration (the best of all samples, $L^*/a^*/b^* = 53/25/29$), in correlation with its higher Tb content. Secondly, the level of homogeneity in Tb distribution within the solid solutions appears also to be an important parameter. Effectively, in samples with a similar Tb content (*i.e.* samples *CONO3-1* and *COCl-HT*, or samples *MW-UR1* and *COOX*), the best red colours appear to be associated to samples with the more homogenous Tb distribution (*COCl-HT* and *COOX*, respectively). Indeed, considering the more heterogeneous samples (COCl, EV-NO3 and CONO3-1) having two distinct cerianite solid solutions (with different Tb content), only EV-NO3 sample presents a nice red colour ($a^* = 21$), while the others give rise to very poor red colours ($a^* = 13$ and 16).

On the other hand, the reflectance curves of all enamelled samples are also shown in Fig. 11. Obviously, and similarly

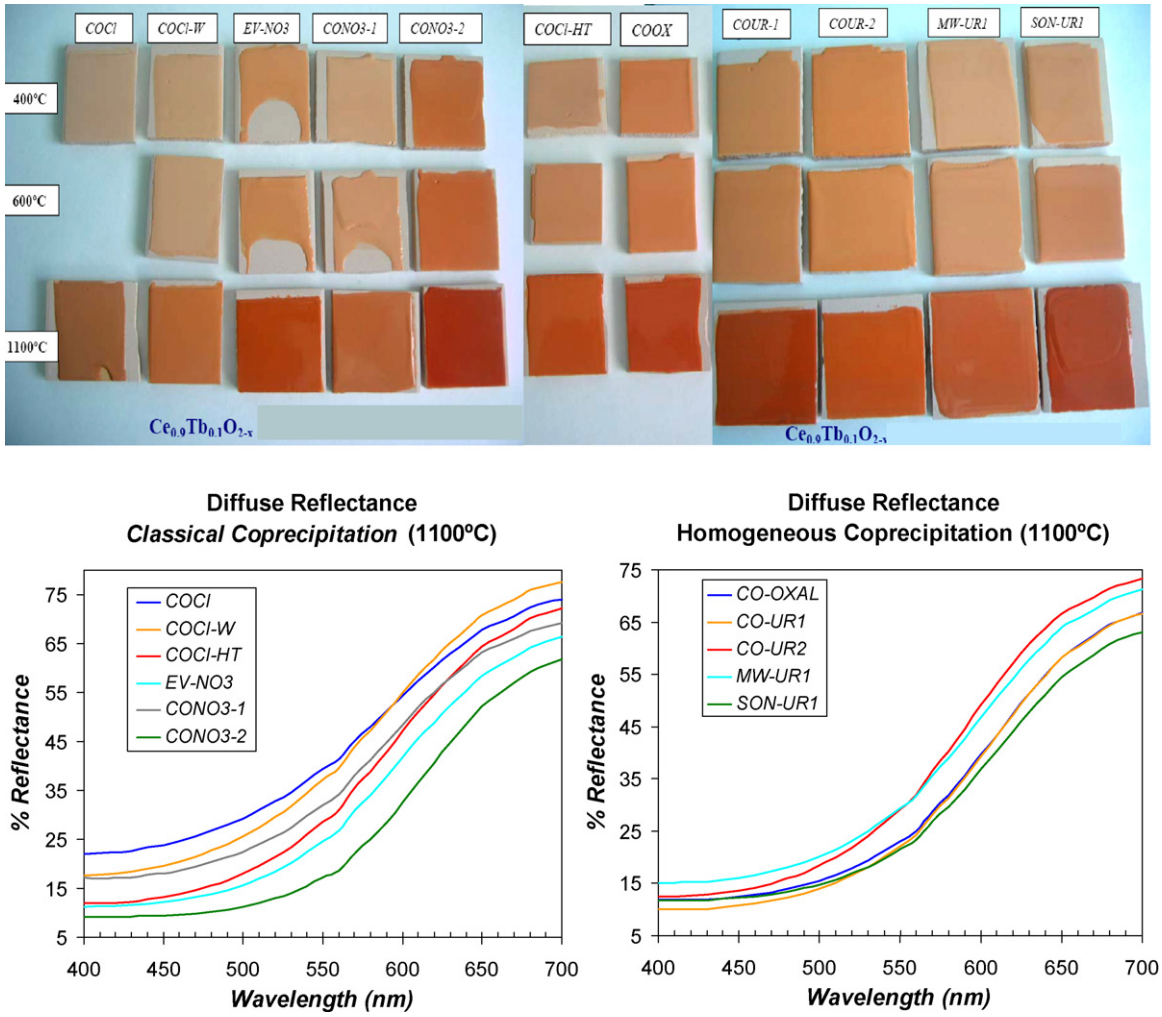

Fig. 11. Aspect of enamelled samples (5 wt% pigment within a conventional double-firing glaze), and corresponding diffuse reflectance spectra of 1100 °C-fired coprecipitate $Ce_{0.9}Tb_{0.1}O_2$ samples (left: classical coprecipitation routes; right: homogeneous coprecipitation routes). (For interpretation of the references to colour in this figure legend, the reader is referred to the web version of this article.)

to the previous compositional study, samples having the best red colours posses the minimum reflectance around 450–500 nm and the maximum reflectance being centred at *ca.* 650–700 nm (red region). From these reflectance curves, the approximate energy bandgap values (E_g, in eV) were also estimated (see Tables 4 and 5). As it may be appreciated in Fig. 12 there is a clear linear (and inverse) tendency between the obtained bandgap values and the resulting red colour (a^* parameter) of enamelled samples. In both classical and homogeneous coprecipitation samples the best red colourations are associated to

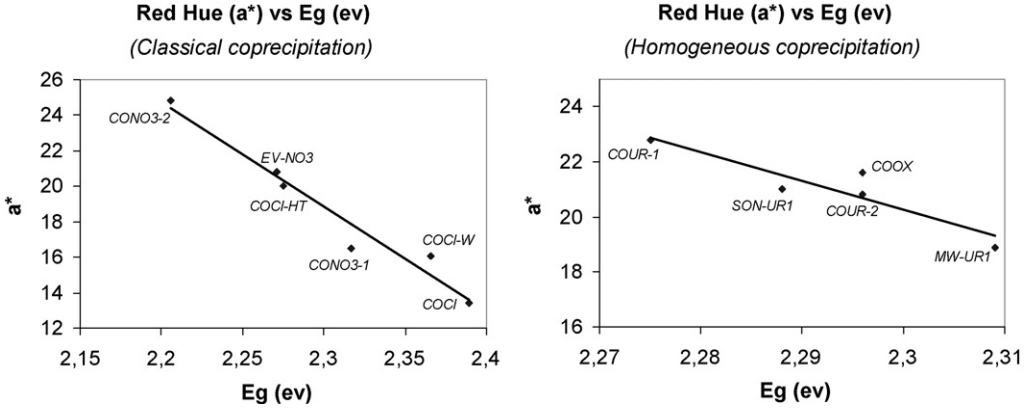

Fig. 12. Representation of the bandgap energy (E_g) *vs* the red colour parameter (a^*) in both *classical* and *homogeneous* coprecipitation samples. An inverse linear correlation is observed.

the lower bandgap values (below 2.30 eV), the best red colour ($a^* = 25$) being presented by sample *CONO3-2* with the lowest bandgap value (2.21 eV).

As general conclusions, firstly it has been herein demonstrated that the employment of coprecipitation methods of higher homogeneity (with oxalates o urea) leads to the formation of more homogeneous solid solutions of CeO_2-Tb. With these routes, the obtained pigments have a Tb content very close to that of the nominal (initial) formulation ($Ce_{0.9}Tb_{0.1}O_2$) and exhibit very nice reddish colourations (except in *MW-UR1*), improving a great deal the colourations accomplished with classical coprecipitation routes (except in *CONO3-2* sample).

Secondly, in the classical coprecipitation route with chlorides the results are a great deal improved with the hydrothermal treatment, and regarding to the three investigated synthesis alternatives with nitrates, the method of "colloid stabilization" (*CONO3-2*) leads to the best red colouration of all samples.

Finally, in the series of homogeneous coprecipitation with urea (and nitrates precursors), the assistance with ultrasounds does not improve results, while the alternative method using microwaves has the clear advantage of the very rapid preparation and energy saving (5–10 min of preparation), but results in a slightly poorer red colour ($a^* = 19$).

5. Conclusions

In this manuscript we have reported about the optimization of the synthesis and colour properties of CeO_2-Tb reddish ceramic pigments. The great interest and novelty of this research lies on the very scarce investigations available in the literature on this system, which are mostly concerned on their catalytic and redox properties. Moreover, any research concerning the development or improvement of ceramic pigments with reddish hues is still a hot topic and one of the main objectives to be accomplished by the ceramic industry. In a preliminary study we have determined the optimal composition of Tb (and Y)-doped CeO_2 solid solutions ($Ce_{0.9}Tb_{0.1}O_{0.2}$), and demonstrated the possibility of obtaining very nice reddish colourations at 1500 °C by the traditional ceramic route. The red colours obtained through the use of the classical coprecipitation route with chlorides precursors were also very intense at 1500 °C, but they were still very poor at lower temperatures (1100 °C).

Consequently, in the second part of this study the effect of using different classical and non-conventional coprecipitation routes on the low-temperature (400–1100 °C) synthesis and colour performance of Tb-CeO_2 red pigments has been analyzed for the first time. Very interestingly, the optimization of synthesis methods has proven to enable the formation of more homogeneous (single phase) CeO_2-Tb solid solutions at lower temperatures, and also to modulate the final Ce–O and Tb–O chemical environments in the pigment (lattice parameters and optical bandgaps), thus improving the final reddish colouration at 1100 °C. The obtained colour parameters of the optimal samples enamelled with a conventional transparent ceramic glaze ($L^*/a^*/b^*$ parameters around 53–59/22–25/29–34) are as good as those previously reported for CeO_2-Pr pigments.[21,32,34,43] Accordingly, the compositions and synthesis methods herein optimized have a clear potential for the production of environmentally friendly reddish ceramic pigments, alternative to CeO_2-Pr ceramic pigments, although at present there is still the inconvenience of the higher price of Tb with respect to Pr. The "colloid stabilization route" with nitrates (*CONO3-2*) and also the homogeneous coprecipitation routes with oxalates and urea (*COOX* and *COUR-1*) appear as the most recommendable synthesis approaches.

Acknowledgements

The authors thank the Spanish "*Ministerio de Educación y Ciencia*" (Project MAT2008-02893) for financial support. Moreover, the technical assistance provided by the Central Services of Scientific Instrumentation (SCIC) of the University Jaume I is also gratefully acknowledged.

Appendix A. Supplementary data

Supplementary data associated with this article can be found, in the online version, at doi:10.1016/j.jeurceramsoc.2009.08.005.

References

1. Rojas, T. C. and Ocaña, M., Uniform nanoparticles of Pr(III)/Ceria solid solutions prepared by homogeneous precipitation. *Scripta Mater.*, 2002, **46**, 655–660.
2. Rajendran, M., Mallick, K. K. and Bhattacharya, A. K., Combustion synthesis, powder characteristics and crystal structure of phases in Ce–Pr–O system. *J. Mater. Sci.*, 1998, **33**, 5001–5006.
3. Mokkelbost, T., Kaus, I., Grande, T. and Einarsrud, M.-A., Combustion synthesis and characterization of nanocrystalline CeO_2-based powders. *Chem. Mater.*, 2004, **16**, 5489–5494.
4. Bernal, S., Blanco, G., Cauqui, M. A., Corchado, P., Pintado, J. M., Rodríguez-Izquierdo, J. M. and Vidal, H., Fundamental properties of a new cerium-based mixed oxide alternative as TWC component. *Stud. Surf. Sci. Catal.*, 1998, **116**, 611–618.
5. Li, X., Peian, L., Wang, W., Yang, Z., Fu, Y. and Yu, S., A novel preparation route of three-way catalysts. *Top. Catal.*, 2001, **16–17**(1–4), 107–113.
6. O'Conell, M. and Morris, M. A., New ceria-based catalysts for pollution abatement. *Catal. Today*, 2000, **59**, 387–393.
7. Zhao, S. and Gorte, R. J., The effect of oxide dopants in ceria on *n*-butane oxidation. *Appl. Catal. A*, 2003, **248**, 9–18.
8. Bryan-Balazs, H. G. and Glass, R. S., ac impedance studies of rare earth oxide doped ceria. *Solid State Ionics*, 1995, **76**, 152–162.
9. Dudek, M., Ceramic oxide electrolytes based on CeO_2-preparation, properties and possibility of application to electrochemical devices. *J. Eur. Ceram. Soc.*, 2008, **28**, 965–971.
10. Hari Prasad, D., Son, J.-W., Kim, B.-K., Lee, H.-W. and Lee, J.-H., Synthesis of nano-crystalline $Ce_{0.9}Gd_{0.1}O_{1.95}$ electrolyte by novel sol–gel thermolysis process for IT-SOFCs. *J. Eur. Ceram. Soc.*, 2008, **28**, 3107–3112.
11. Bernal, S., Blanco, G., Botana, F. J., Gatica, J. M., Pérez-Omil, J. A., Pintado, J. M., Rodríguez-Izquierdo, J. M., Maestro, P. and Braconnier, J. J., Study of the reduction/reoxidation cycle in a La/Ce/Tb mixed oxide. *J. Alloys Compd.*, 1994, **207–208**, 196–200.
12. Rhône Poulenc, French Patent 1.257.078, 1960.
13. Llusar, M., Badenes, J. A., Calbo, J., Tena, M. A. and Monrós, G., Environmental optimization of flux additions. *Am. Ceram. Soc. Bull.*, 1999, **78**, 63–68.
14. Llusar, M., Badenes, J. A., Vicent, J. B., Tena, M. A. and Monrós, G., Environmental optimisation of blue vanadium zircon ceramic pigment. *J. Eur. Ceram. Soc.*, 1999, **19**, 2647–2657.

15. Jansen, M. and Letschert, H. P., Inorganic yellow–red pigments without toxic metals. *Nature*, 2000, **404**, 980–982.
16. Fores, A., Llusar, M., Badenes, J. A., Calbo, J., Tena, M. A. and Monrós, G., Cobalt minimisation in willemite ($Co_xZn_{2-x}SiO_4$) ceramic pigments. *Green Chem.*, 2000, **2**(3), 93–100.
17. Furukawa, S., Masui, T. and Imanaka, N., Synthesis of new environmentally friendly yellow pigments. *J. Alloys Compd.*, 2006, **418**, 255–258.
18. Sreeram, K.-J., Srinivasan, R., Devi, J.-M., Fair, B.-U. and Ramasami, T., Cerium molybdenum oxides for environmentally benign pigments. *Dyes Pigments*, 2007, **75**, 687–692.
19. Šulcová, P., Trojan, M. and Šolc, M., Cerium dioxide fluorite type pigments. *Dyes Pigments*, 1998, **37**, 65–70.
20. Šulcová, P. and Trojan, M., Synthesis of $Ce_{1-x}Pr_xO_2$ pigments with other lanthanides. *Dyes Pigments*, 1998, **40**, 87–91.
21. García, A., Llusar, M., Calbo, J., Tena, M. A. and Monrós, G., Low-toxicity red ceramic pigments for porcelainised stoneware from lanthanide-ceria solid solutions. *Green Chem.*, 2001, **3**, 238–242.
22. George, G., Rao, P.-P. and Reddy, M.-L., Synthesis and characterization of CeO_2-TiO_2-Pr_6O_{11} solid solutions for environmentally benign nontoxic red pigments. *Chem. Lett.*, 2006, **35**, 1412–1413.
23. Rao, P.-P. and Reddy, M. L. P., $(TiO_2)_1$ $(CeO_2)_{1-x}$ $(RE_2O_3)_x$—novel environmental secure pigments. *Dyes Pigments*, 2007, **73**, 292–297.
24. Kumari, L.-S., George, G., Rao, P.-P. and Reddy, M. L. P., The synthesis and characterization of environmentally benign praseodymium-doped $TiCeO_4$ pigments. *Dyes Pigments*, 2008, **74**, 427–431.
25. Costa, A. L., Matteucci, F., Dondi, M., Zama, I., Albonetti, S. and Baldi, G., Heterocoagulation-spray drying process for the inclusion of ceramic pigments. *J. Eur. Ceram. Soc.*, 2008, **28**, 169–176.
26. Lavilla, V. L. and López-Rincón, J. M., Study of the mechanism of formation of a zircon–cadmium sulphoselenide pigment. *Britt. Ceram. Trans.*, 1981, **80**, 105–108.
27. OLazcuaga, R., El Kira, A., Le Flem, G. and Hagenmuller, P., Sur des Nouveaux Pigments Rouges de Type Perovskite stables à Haute Température. *Rev. Chim. Minér.*, 1984, **21**, 221–228.
28. Baldi, D. and Dolen, N., Synthesis of a new class of red pigments based on perovskite type lattice for use in body stain and high temperature glazes. *Int. Ceram. J. (Suppl. Ceram. Informazione, Faenza)*, 2000, **4**(April 31), 31–37.
29. Matteucci, F., Cruciani, G., Dondi, M., Baldi, G. and Barzanti, A., Colouring mechanism of red ceramic pigments based on perovskite structure. *Key Eng. Mater.*, 2004, **264–268**, 1549–1552.
30. Llusar, M., Calbo, J., Badenes, J. A., Tena, M. A. and Monrós, G., Synthesis of iron zircon coral by coprecipitation routes. *J. Mater. Sci.*, 2001, **36**, 153–163.
31. Olazcuaga, R., Le Polles, G., El Kira, A., Le Flem, G. and Maestro, P., Optical properties of $Ce_{1-x}Pr_xO_2$ powders and their applications to the coloring of ceramics. *J. Sol. State Chem.*, 1987, **71**, 570–573.
32. Olazcuaga, R., Le Flem, G. and Alarcon, Evolución cromática del pigmento $Ce_{0.95}Pr_{0.05}O_2$: del rojo al amarillo. *Bol. Soc. Esp. Ceram. Vidrio*, 1993, **32**(4), 251–254.
33. Bondioli, F., Bonamartini-Corradi, A. and Manfredini, T., Nonconventional synthesis of praseodymium-doped ceria by flux method. *Chem. Mater.*, 2000, **12**, 324–330.
34. Masó, N., Beltrán, H., Muñoz, R., Julián, B., Carda, J. B., Escribano, P. and Cordoncillo, E., Optimization of praseodymium-doped cerium pigment synthesis temperature. *J. Am. Ceram. Soc.*, 2003, **86**, 425–430.
35. Olazcuaga, R., El Kira, A., Le Flem, G. and Maestro, P., Stabilization of tetravalent praseodymium in cerium oxide (CeO_2): application as stable red pigments at high temperature. *C. R. Acad. Sci. Paris*, 1986, **303**, 361–363.
36. Chaminade, J. P., Olazcuaga, R., Le Polles, G., Le Flem, G. and Hagenmuller, P., Crystal growth and characterization of $Ce_{1-x}Pr_xO_2$ ($x \cong 0.05$) single crystals. *J. Cryst. Growth*, 1988, **87**, 463–465.
37. Aruna, S. T., Ghosh, S. and Patil, K. C., Combustion synthesis and properties of $Ce_{1-x}Pr_xO_{2-\delta}$ red ceramic pigments. *Int. J. Inorg. Mater.*, 2001, **3**, 387–392.
38. López-Navarrete, E., Caballero, A., González-Elipe, A. R. and Ocaña, M., Low-temperature preparation and structural characterization of Pr-doped ceria solid solutions. *J. Mater. Res.*, 2002, **17**, 797–804.
39. Zhu, Z. F., Zhou, Y. and Wang, R. L., Coloring mechanism of Pr-CeO_2 nano-crystalline red lanthanide pigments prepared by low-temperature combustion synthesis. *Key Eng. Mater.*, 2007, **336–338**, 2068–2070.
40. Bondioli, F., Ferrari, A. M., Lusvarghi, L., Manfredini, T., Nannarone, S., Pasquali, L. and Selvaggi, G., Synthesis and characterization of praseodymium-doped ceria powders by a microwave-assisted hydrothermal (MH) route. *J. Mater. Chem.*, 2005, **15**, 1061–1066.
41. Bondioli, F., Ferrari, A. M., Leonelli, C., Siligardi, C., Neil, A. H. and Evans, G., The application of microwaves in the synthesis of $Ce_{0.9}Pr_{0.1}O_2$ nanostructured powders. *J. Mater. Chem.*, 2005, **15**, 1061–1066.
42. Olazcuaga, R., Le Flem, G. and Alarcon, J., Introduction of Tb^{4+} into CeO_2 to obtain stable red pigments at high temperatures. *Bol. Soc. Esp. Ceram. Vidrio*, 1993, **32**(5), 307–310.
43. García, A., Llusar, M., Calbo, J., Mestre, A., Tena, M. A. and Monrós, T., Optical effects of the inclusion of lanthanides in ceria lattice. In *Actas del XII Simposio del Grupo Especializado de Cristalografía (Perspectivas de la cristalografía ante el nuevo milenio)*, ed. V. Esteve and L. E. Ochando. Gráficas Uncilla, Castellón, 2001, pp. 113–122.
44. Dixit, M., Subbanna, G. N. and Kamath, P. V., Homogeneous precipitation from solution by urea hydrolysis: a novel chemical route to the α-hydroxides of nickel and cobalt. *J. Mater. Chem.*, 1996, **6**, 1429–1432.
45. García, A., Calbo, J., Sorlí, S., Bedoya, D., Llusar, M., Badenes, J. and Tena, M. A., Synthesis of hematite-zircon ceramic pigment by urea homogeneous coprecipitation. In *CIMTEC 2002-10th international ceramics congress (international symposium "Science for new technology of silicate ceramics")*, ed. P. Vincenzini and M. Dondi, 2003, pp. 287–298.
46. Rao, K. J., Vaidhyanathan, B., Ganguli, M. and Ramakrishnan, Synthesis of inorganic solids using microwaves. *Chem. Mater.*, 1999, **11**, 882–895.
47. Suslick, K. S., Fang, M. and Hyeon, T., Sonochemical synthesis of iron colloids. *J. Am. Chem. Soc.*, 1996, **118**, 11960–11961.
48. Xiao, Q., Huang, S., Zhang, J., Xiao, C. and Tan, X., Sonochemical synthesis of ZnO nanosheet. *J. Alloys Compd.*, 2008, **459**, L18–L22.
49. Jevtić, M. and Uskojović, D., Influence of urea as a homogeneous precipitation agent on sonochemical hydroxyapatite synthesis. *Mater. Sci. Forum*, 2007, **555**, 285–290.
50. Suslick, K. S., Didenko, Y., Fang, M. M., Hyeon, T., Kolbeck, K. J., McNamara III, W. B., Mdleleni, M. M. and Wong, M., Acoustic cavitation and its chemical consequences. *Phil. Trans. R. Soc. Lond. A*, 1999, **357**, 335–353.
51. Calbo, J., Gargori, C., Sorlí, S., Badenes, J., Tena, M. A. and Monrós, G., Síntesis de pigmentos cerámicos mediante radiación microondas. *Bol. Soc. Esp. Ceram. Vidrio*, 2007, **46**(1), 14–20.
52. Lai, T.-L., Lai, Y.-L., Lee, C.-C., Shu, Y.-Y. and Wang, C.-B., Microwave-assisted rapid fabrication of Co_3O_4 nanorods and application to the degradation of phenol. *Catal. Today*, 2008, **131**, 105–110.
53. Werner, P.-E., Eriksson, L., Westdahl, M. and TREOR, a semi-exhaustive trial-and-error powder indexing program for all symmetries. *J. Appl. Crystallogr.*, 1985, **18**, 367–370.
54. Win-metric®, Siemens analytical X-ray systems, Reg. Trademark of Sigma-C.
55. García, A., Sorlí, S., Mestre, A., Badenes, J., Tena, M. A. and Monrós, G., Interacción reactiva esmalte-color. Control de la desgasificación con pigmentos de base cerianita. In *Proceedings of Qualicer 2002 (VII Congreso Mundial de la calidad del azulejo y del pavimento cerámico), vol. III*, 2002, pp. pos23–pos27.
56. Llusar, M., Forés, A., Badenes, J. A., Calbo, J., Tena, M. A. and Monrós, G., Colour analysis of some cobalt-based blue pigments. *J. Eur. Ceram. Soc.*, 2001, **21**, 1121–1130.
57. CIE, Recommendations on uniform colour spaces, colour difference equations, psychometrics colour terms. In *Suplement no. 2 of CIE Publ. No. 15 (E1-1.31), 1971*. Bureau Central de la CIE, Paris, 1978.